JOURNAL OF MATERIALS SCIENCE 31 (1996) 1715–1724

The effect of $MgAl_2O_4$ on the formation kinetics of Al_2TiO_5 from Al_2O_3 and TiO_2 fine powders

V. BUSCAGLIA, M. ALVAZZI DELFRATE, M. LEONI, C. BOTTINO
Istituto di Chimica Fisica Applicata dei Materiali, Consiglio Nazionale delle Ricerche, via De Marini 6, I-16149 Genoa, Italy

P. NANNI
Istituto di Chimica, Facoltà di Ingegneria, Fiera del Mare, Piazzale Kennedy, Pad. D, I-16129 Genoa, Italy

The formation of $Al_{2(1-x)}Mg_xTi_{(1+x)}O_5$ solid solutions from Al_2O_3–TiO_2–$MgAl_2O_4$ powder mixtures of ≈ 1 μm particle size and moderate purity has been studied at 1300 °C for different final composition values: $x=0$ ("pure" Al_2TiO_5), 10^{-3}, 10^{-2} and 10^{-1}. Analysis of the kinetic data and microstructural observation indicates that $MgAl_2O_4$ affects the mechanism of Al_2TiO_5 formation by providing active nuclei for the growth of the new phase. These nuclei are probably constituted by $Mg_{0.5}AlTi_{1.5}O_5$, i.e. the equimolar Al_2TiO_5–$MgTi_2O_5$ solid solution, and are formed by reaction between $MgAl_2O_4$ and TiO_2 at temperatures above ≈ 1150 °C. As the value of x increases, the number of titanate particles per unit volume accordingly increases and the conversion of the original oxides is faster. At values of $x \leqslant 10^{-2}$, the prevailing mechanism is the nucleation and growth of Al_2TiO_5 nodules for fractional conversion up to ≈ 0.8. Further conversion of the residual Al_2O_3 and TiO_2 particles dispersed into the titanate nodules is slower and controlled by solid-state diffusion through Al_2TiO_5. At $x=0.1$, a large number of nucleation sites is present, and solid-state diffusion through Al_2TiO_5 becomes important even in the initial stage of reaction, as the diffusion distances are strongly reduced. The study of Al_2TiO_5 formation under non-isothermal conditions in the temperature range 1250–1550 °C shows that reaction proceeds between 1300 and 1350 °C for $x=0.01$ and between 1250 and 1300 °C for $x=0.1$. Densification of the titanate becomes important at temperatures above 1300 °C for $x=0.1$, but only above 1450 °C for $x=0.01$.

1. Introduction

Aluminium titanate is a promising ceramic for technological applications due to its very low thermal expansion coefficient, low thermal conductivity and excellent thermal shock resistance [1]. This material is conventionally prepared by reaction sintering of Al_2O_3 and TiO_2 powders. Above 1280 °C [2], formation of Al_2TiO_5 occurs in an oxidizing atmosphere according to

$$\alpha\text{-}Al_2O_3 + TiO_2\text{-rutile} \rightarrow \beta\text{-}Al_2TiO_5 \quad (1)$$

where the phases present are those which are thermodynamically stable. Below 1280 °C, aluminium titanate decomposes, as it is unstable in comparison to Al_2O_3 and TiO_2. The kinetics of Reaction 1 has been carefully investigated by Freudenberg and Mocellin [3, 4]. Depending on temperature and on advancement of the reaction, different overall reaction kinetics and microstructure evolution have been observed.

In the range 1280–1400 °C, the chemical driving force (proportional to the difference T-1280, where T is the experimental temperature) is too small in comparison with the strain energy associated with bulk nucleation of the new phase. As a consequence, titanate formation can start only at a limited number of "easy-to-nucleate" sites with growth of quite large Al_2TiO_5 crystals. The growth rate is controlled by the rapid bulk or interface transport of aluminium ions through TiO_2-rutile. This fast growth interrupts at a fractional conversion < 1, when the entire sample volume is completely occupied. The titanate-forming reaction continues at a reduced rate, as the conversion of the residual Al_2O_3 and TiO_2 particles dispersed into the Al_2TiO_5 cells is controlled by slower solid-state diffusion through Al_2TiO_5. The final microstructure of the sintered body is therefore porous and large-grained (≈ 100 μm), even though the average grain size strongly depends on the level and the nature of impurities present in the starting materials [5]. At $T > 1400$ °C, a large number of nucleation sites becomes available and the reactants are quasi-immediately separated by the forming new phase; the growth rate is controlled by solid-state diffusion through the Al_2TiO_5 layer.

Several additives, such as SiO_2 [6], ZrO_2 [6, 7], Fe_2O_3 [8] and MgO [6, 9] have been added to control

0022–2461

the thermal decomposition of Al_2TiO_5 below 1280 °C and to increase the poor mechanical strength related to the extensive microcracking in sintered polycrystals. Only Fe_2O_3 and MgO seem to offer an improved and reliable phase stability and this ability is related to the formation of solid solutions between Al_2TiO_5 and the isostructural Fe_2TiO_5 and $MgTi_2O_5$ compounds. In previous papers [10, 11], the effect MgO addition on the reactive sintering of Al_2TiO_5 from rutile and α-alumina was investigated. The final materials, $Al_{2(1-x)}Mg_xTi_{(1+x)}O_5$ solid solutions with x ranging from 0.01–0.2, exhibit high density (95%) and relatively small grains (5–10 μm). The importance of the nucleation process of the new phase on the resulting microstructure was identified. Initially, MgO reacts with Al_2O_3 to form spinel

$$MgO + Al_2O_3 \rightarrow MgAl_2O_4 \quad (2)$$

This reaction occurs below 1100 °C and determines the complete conversion of MgO. At $T \approx 1200$ °C, the formation of a solid solution $Al_{2(1-x)}Mg_xTi_{(1+x)}O_5$ with $x > 0.2$ was observed and it was suggested that titanate formation begins with the solid solution with $x = 0.5$ according to

$$\tfrac{1}{2}MgAl_2O_4 + \tfrac{3}{2}TiO_2 \rightarrow AlMg_{0.5}Ti_{1.5}O_5 \quad (3)$$

As temperature further increases, the composition of the solid solution approaches the final one. It was proposed that the magnesium-rich titanate crystals initially formed, therefore act as preferential sites for further titanate nucleation and growth, producing the observed dense and fine-grained microstructure.

In the present work, the formation kinetics of Al_2TiO_5 from the parent oxides in the presence of different amounts of $MgAl_2O_4$, corresponding to x in the solid solution ranging from 0.001 to 0.1, was investigated at $T = 1300$ °C. The variation of x should provide a different number of active nuclei for titanate growth, resulting in different kinetic behaviours and different final microstructures. The results should also give useful information about the origin of the "easy-to-nucleate" sites which plays an important role in the formation of aluminium titanate [3, 5].

2. Experimental procedure

Different mixtures of α-Al_2O_3 (Keramont 100PCT/TLV/TWA, 99.99%, $X_{50} = 0.5$ μm), TiO_2 (Aldrich 22 422-7, predominantly rutile, 99.9%, $X_{50} = 1$ μm) and $MgAl_2O_4$ (obtained by firing at 1400 °C a mixture of MgO (Aldrich 34 279-3, 99%) and the same alumina used to prepare the titanate, particle size 0.2–1 μm) corresponding to $x = 0$, 10^{-3}, 10^{-2} and 0.1 in $Al_{2(1-x)}Mg_xTi_{(1+x)}O_5$, were prepared by mixing and wet-milling in distilled water for 24 h using alumina balls and PE bottles. The resulting powders, after drying and sieving, were isostatically pressed at 150 MPa forming cylinders of ≈ 10 mm diameter and ≈ 100 mm length. The green density, determined by geometry and weight, was 2.0–2.1 g cm^{-3}. The chemical analysis of the main impurities of the as-milled powder without $MgAl_2O_4$ addition is shown in Table I. Silicon, sodium and calcium are the primary contaminants. The kinetics of Reaction 1 was investigated at $T = 1300$ °C for times ranging from 5 min to 16 h. The experimental temperature was chosen slightly higher than that reported for Al_2TiO_5 formation (1280 °C [2]) in that the addition of spinel increases the reaction rate and the initial stages of the reaction could not be observed at higher temperatures. In the case for $x = 0.01$, the reaction kinetics was also measured on samples presintered at 1100 °C for 24 h. Initial densities of 2.3–2.4 g cm^{-3} have thus been obtained. In order to study the occurrence of Reaction 3, stoichiometric mixtures of $MgAl_2O_4$ and TiO_2 were prepared following the procedure above reported and fired at 1200 and 1300 °C for times ranging from 10 min to 8 h. All the kinetic experiments were carried out in air using slices ≈ 1 cm thick cut from the green cylinders. To reduce the influence of heating time, the samples were put inside the furnace, kept at a preset temperature, within 30 s. The samples reached the firing temperature in ≈ 3 min. The temperature through the hot zone, measured by a S-type thermocouple, was constant within ± 3 °C. The experimental time being expired, the samples were pulled out of the furnace and air-quenched. Reaction times shorter than 5 min were avoided to reduce experimental errors. The relative amount of titanate solid solution after reaction was measured after fine grinding in an agate mortar by quantitative X-ray diffraction (XRD, Philips PW1710/PW1050/PW1729, CoK_α radiation, secondary graphite monochromator). The scanning step was 0.025° 2θ and the sampling time 5 s for each point, with digital collection of the resulting pattern.

TABLE I Chemical analysis (p.p.m.) of Al_2O_3/TiO_2 equimolar mixture by ICP spectroscopy

SiO_2	Na_2O	CaO	Fe_2O_3	MgO	ZrO_2
800	920	810	120	200	35

For mixtures with $x \leqslant 0.01$, the amount of $MgAl_2O_4$ present in the reacted samples is practically undetectable and the following system of linear equations was used to determine the concentration of α-Al_2O_3, TiO_2-rutile, and Al_2TiO_5

$$\frac{I_{Al_2TiO_5(023)}}{I_{TiO_2(110)}} = C\frac{W_{Al_2TiO_5}}{W_{TiO_2}} \quad (4a)$$

$$\frac{n_{Al_2O_3}}{n_{TiO_2}} = 1 \quad (4b)$$

$$W_{Al_2O_3} + W_{TiO_2} + W_{Al_2TiO_5} = 1 \quad (4c)$$

where $I_{Al_2TiO_5(023)}$ is the intensity of the (0 2 3) reflection of Al_2TiO_5, $I_{TiO_2(110)}$ the intensity of the (1 1 0) reflection of rutile, W_i the weight fraction, n_i the number of moles and C a constant dependent on the crystal structure and lattice parameters of Al_2TiO_5 and rutile. The value of C calculated from available structural data [12–14] is 0.36. The measure of integrated intensity was preferred over the measure of the peak height to avoid effects arising from milling time and annealing. The entire diffraction pattern in the range

$d = 5.15$–2.12 was fitted by a linear combination of pseudo-Voigt functions to describe the peaks profile and a straight line for the background. The area of each peak, i.e. the integrated intensity, results then as a function of some adjustable parameters. The adjustable parameters were calculated by minimizing the chi-square function. To test the validity of the method described by Equations 4a–c, different standards containing, respectively 5, 10, 20, 40, 60 and 80 wt % Al_2TiO_5 where prepared. The ratio $I_{Al_2TiO_5(023)}/I_{TiO_2(110)}$ was plotted against the ratio $W_{Al_2TiO_5}/W_{TiO_2}$. The data are described by a straight line, and regression analysis gives a slope of 0.35 ± 0.01, in good agreement with the theoretical value. The reproducibility of the results was investigated by determining the composition of different samples reacted for the same time. The minimum detectable level of Al_2TiO_5 was 0.5–1 wt %.

For mixtures with $x = 0.1$, the presence of $MgAl_2O_4$ can no longer be neglected. In addition, a complication arises from the formation of magnesium-richer solid solutions in the initial stages of the reaction. The current value of x in the solid solution can be determined from the cell constants of the new phase, assuming a linear dependence on the composition, as previously reported [6]. The composition of the mixture is then given by resolution of the following system of linear equations

$$\frac{I_{Al_2TiO_5(023)}}{I_{TiO_2(110)}} = C_1 \frac{W_{Al_2TiO_5}}{W_{TiO_2}} \quad (5a)$$

$$\frac{I_{Al_2O_3(012)}}{I_{TiO_2(110)}} = C_2 \frac{W_{Al_2O_3}}{W_{TiO_2}} \quad (5b)$$

$$\frac{I_{MgAl_2O_4(311)}}{I_{TiO_2(110)}} = C_3 \frac{W_{MgAl_2O_4}}{W_{TiO_2}} \quad (5c)$$

$$W_{TiO_2} + W_{Al_2O_3} + W_{MgAl_2O_4} + W_{Al_2TiO_5} = 1 \quad (5d)$$

where the different symbols have the same meaning as in Equations 4a–c. The subscript Al_2TiO_5 now indicates the Al_2TiO_5–$MgTi_2O_5$ solid solution at variable composition, and the value of C_1 is computed according to the actual composition. Because, for times longer than 20 min, the residual spinel is below the XRD detection limit, the problem can be reduced to resolution of Equations 5a, b and d by setting $W_{MgAl_2O_4} = 0$. A system of equations similar to Equations 4a–c was also used in the case of Reaction 3.

Microstructure was observed by optical (OM, Reichert) and scanning electron microscopy (SEM, Philips 515) after infiltration of the specimen in epoxy resin and the usual metallographic preparation. The backscatter (BS) mode was especially useful to distinguish the different phases, which appear white (TiO_2), dark grey (Al_2O_3) and intermediate grey (Al_2TiO_5). The microstructure of reacted samples was characterized by image analysis (analySIS).

Kinetic experiments were also performed under non-isothermal conditions. Samples were heated up to temperatures between 1250 and 1550 °C, with 50 °C intervals, at 1 °C min^{-1}. As soon as the preset temperature was reached, the samples were cooled down rapidly. The phases present were determined by X-ray diffraction. The final density was measured by a water-immersion method, coating the specimens with a thin gloss layer to avoid water absorption.

3. Results and discussion

3.1. Al_2TiO_5 isothermal formation kinetics

The isothermal reaction kinetics (Al_2TiO_5 weight fraction) $\alpha = f(t)$ at 1300 °C is reported in Fig. 1 for different values of the final composition parameter x: 0, 10^{-3}, 10^{-2} and 10^{-1}. The conversion rate is strongly dependent on the amount of $MgAl_2O_4$ present. The curve at $x = 10^{-3}$ is very close to that corresponding to the formation of "pure" Al_2TiO_5; such a small value has been chosen to increase the level of "magnesium impurities" in the moderate purity reacting mixture. The amount of added spinel corresponds to about 200 p.p.m. MgO in the mixture, a value comparable with the amount of MgO present in the starting powders. As a consequence, the effective final composition will corresponds to $x \approx 2 \times 10^{-3}$. An incubation period of about 30–40 min exists before the Al_2TiO_5 fraction reaches approximately 1%. During this time the sample undergoes an important densification, according to previous dilatometric experiments [5, 10], and $\approx 90\%$ of the ultimate density is reached. As a consequence, it can be assumed that Al_2TiO_5 formation occurs in a matrix of approximately constant density. The incubation period is strongly reduced at $x = 0.01$, where the reacted fraction reaches $\approx 10\%$ after 5 min for standard samples and $\approx 2\%$ after 10 min for presintered samples. The early formation of titanate inhibits the initial densification of the Al_2O_3/TiO_2 mixture and the reaction occurs in a porous matrix. The initially formed Al_2TiO_5 particles generally show a spherical shape and contain Al_2O_3 and TiO_2 inclusions, as shown in Fig. 2. At $x = 0.1$ the conversion is so fast that the initial stages of the reaction cannot be observed; the reaction is $\approx 70\%$ completed after 5 min. For $x \leqslant 0.01$, when the converted fraction exceeds about 80%, the reaction rate strongly decreases and further formation of Al_2TiO_5 occurs slowly. After 16 h reaction, about 10% of unreacted oxides are still present. On the contrary, for $x = 0.1$ the reaction is practically complete after 2 h (96% conversion). Comparison between the microstructure developed in samples with

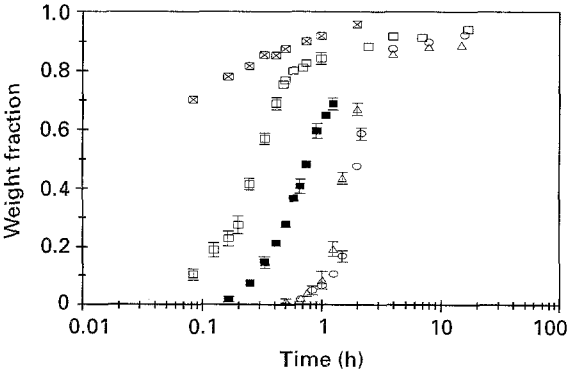

Figure 1 Reaction kinetics at 1300 °C. x: (○) 0, (△) 0.001, (□) 0.01, (■) 0.01 presintered, (⊠) 0.1.

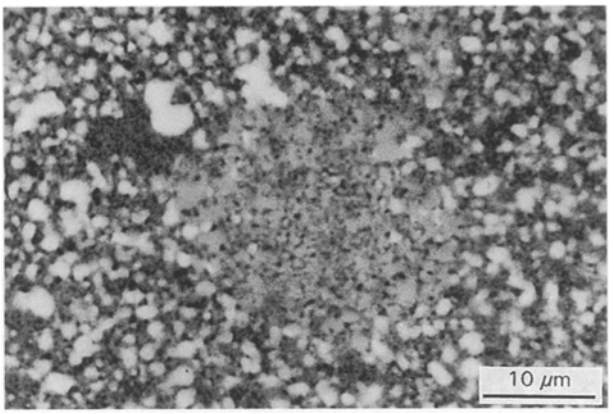

Figure 2 Al_2TiO_5 single nodule formed in a sample with composition $x = 0$ reacted 40 min at 1300 °C (SEM/BS).

$x = 0$ and $x = 0.01$ at different values of the converted fraction α is presented in Fig. 3a–f. Initially the reaction occurs by the growth of isolated Al_2TiO_5 nodules (Fig. 3a and b) into a fine-grained Al_2O_3/TiO_2 matrix. The formation of a larger number of smaller Al_2TiO_5 nodules at $x = 0.01$ in comparison to $x = 0$ is evident. As the reaction proceeds, the titanate crystals grow further (Fig. 3c and d) and impinge into each other. The growth terminates when the sample volume is completely filled (Fig. 3e and f). This point corresponds to a converted fraction $\alpha \approx 0.8$. Further reaction leading to the conversion of Al_2O_3 and TiO_2 residual particles can only proceed by solid-state diffusion through the Al_2TiO_5 matrix, corresponding to the second, slow, reaction stage observed in Fig. 1. The coarsening of Al_2O_3 and TiO_2 particles due to

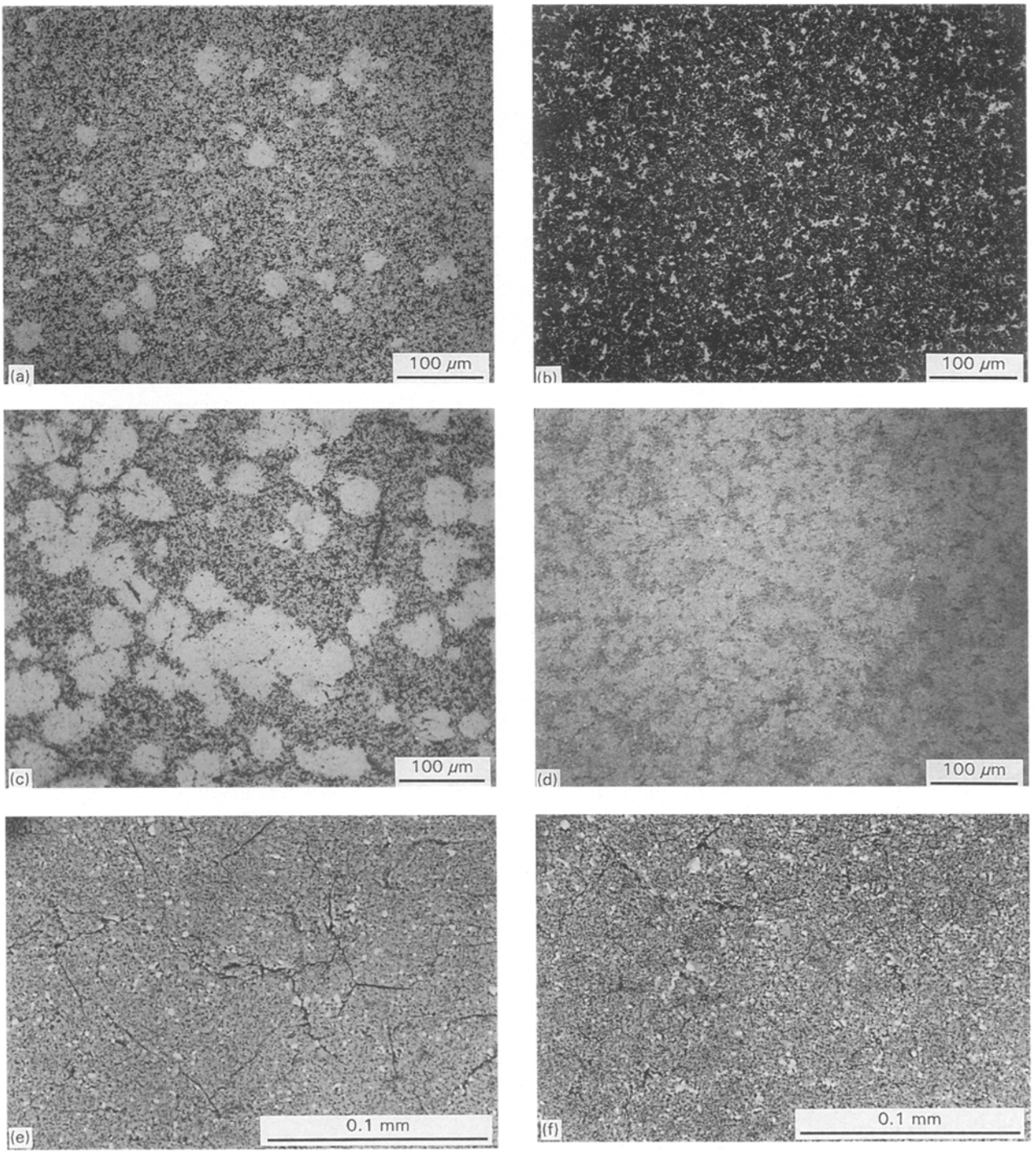

Figure 3 Growth of Al_2TiO_5 particles into the Al_2O_3–TiO_2 fine matrix: (a) $x = 0$, 1 h, $\alpha = 0.05$; (b) $x = 0.01$, 5 min, $\alpha = 0.1$; (c) $x = 0$, 2 h, $\alpha = 0.47$; (d) $x = 0.01$, 20 min, $\alpha = 0.57$; (e) $x = 0$, 4 h, $\alpha = 0.87$; (f) $x = 0.01$, 1 h, $\alpha = 0.84$; (a–d) OM; (e, f) SEM/BS.

Ostwald ripening contributes in slowing down the kinetics, as both the particle size and the diffusion distance increase with time. In the case for $x = 0.1$, after 5 min reaction, the microstructure (Fig. 4) shows a matrix of quite fine Al_2TiO_5 particles (0.5–3 μm) containing many particles of residual TiO_2, probably corresponding to the biggest original particles and some small aggregates of Al_2O_3.

From the kinetic and microstructural observations it can be concluded that the formation of Al_2TiO_5 becomes increasingly fast as the value of x increases, probably due to the presence of a larger number of nucleation centres associated with the $MgAl_2O_4$ seeds. Addition of as little as 10^{-2} mol % $MgAl_2O_4$ is sufficient practically to suppress the induction period, but titanate formation still occurs by two different mechanisms, as already observed for pure Al_2TiO_5 [3, 4]. At higher $MgAl_2O_4$ content ($x = 0.1$) an important contribution of mass transport through Al_2TiO_5 in the overall reaction mechanism is expected, as indicated by the small size of the titanate particles and the almost complete conversion achieved in ≈ 2 h.

3.2. Growth kinetics

The sigmoidal shape of the $\alpha = f(t)$ curves of Fig. 1 corresponding to $x = 0$, 10^{-3} and 10^{-2}, is typical of nucleation and growth processes and data can be tentatively analysed using the Johnson–Mehl–Avrami phenomenological equation

$$\beta(t) = 1 - \exp(-kt^m) \quad (6)$$

where β is the volume fraction reacted in a time t, m and k are two constants. The physical meaning of m and k is related to the boundary conditions of the nucleation and growth process; in particular, the value of m depends on the nature of the nucleation site and on the growth-controlling mechanism [15]. Equation 6 can be linearized writing

$$\ln \ln\left(\frac{1}{1-\beta}\right) = \ln k + m \ln t \quad (7)$$

Because the sample volume is completely filled ($\beta = 1$) by Al_2TiO_5 crystals when $\alpha \approx 0.8$, the reacted fraction α has been multiplied by a factor 1.25 to obtain the corresponding β value. The so corrected data are plotted according to Equation 7 in Fig. 5. A linear regression analysis of the data yields the values of m and k reported in Table II together with the corresponding standard deviations.

3.2.1. Samples with composition $x = 0$ and 10^{-3}

At $x = 0$ and 10^{-3}, $m = 3.2$ and 3.4, respectively. These values are close to the theoretical value $m = 3$, typical of processes where all nucleation centres are exhausted at an early stage of the reaction (zero nucleation rate) and constant growth rate [15]. This result is consistent with the conclusions of Freudenberg and Mocellin [3]. Even though the curves of Fig. 4 corresponding to $x = 0$ and 10^{-3} are very close, regression analysis shows a little, but significant difference between the k values: $1.9 \times 10^{-12}\,s^{-3}$ at $x = 0$ and $3.1 \times 10^{-12}\,s^{-3}$ at $x = 10^{-3}$. This difference may be referred to additional nucleation sites created by the $MgAl_2O_4$ particles, if the growth rate is assumed constant. The kinetic constant k, when $m = 3$, can be expressed as [15]

$$k = \tfrac{4}{3}\pi N_0 u^3 \quad (8)$$

where N_0 is the initial density of the nuclei and u is the

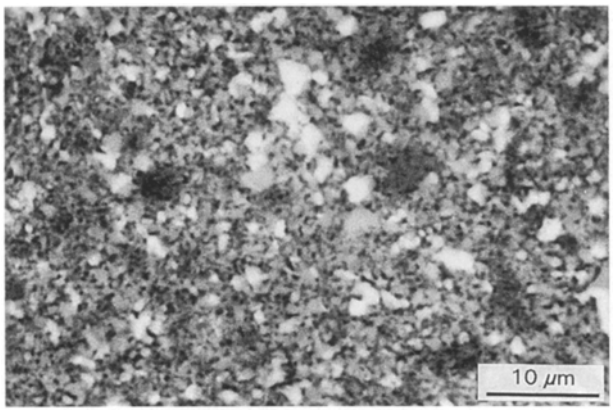

Figure 4 Microstructure of a sample with final composition $x = 0.1$ reacted 5 min at 1300 °C (SEM/BS).

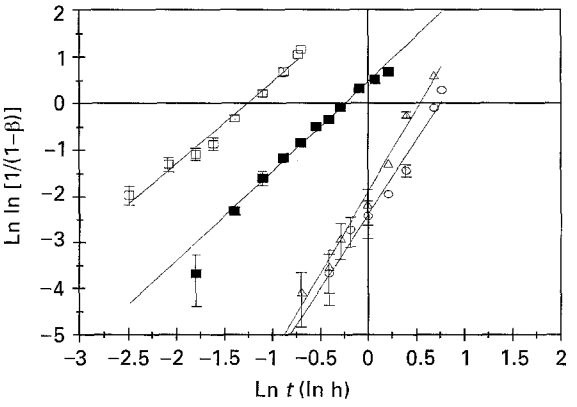

Figure 5 Avrami plot of the kinetic data corresponding to Fig. 1. x: (○) 0, (△) 0.001, (□) 0.01, (■) 0.01 presintered.

TABLE II Parameters m and k from least squares fit of the kinetic data with the Avrami equation $\beta(t) = 1 - \exp(-kt^m)$

	x				
	0	0.001	0.01	0.01 presintered	0.1
m	3.2 ± 0.3	3.4 ± 0.3	1.7 ± 0.1	1.9 ± 0.1	0.29
k	$1.9 \pm 0.6 \times 10^{-12}$ (s^{-3})	$3.1 \pm 0.8 \times 10^{-12}$ (s^{-3})	$4.2 \pm 1 \times 10^{-5}$ ($s^{-3/2}$)	$1.2 \pm 0.3 \times 10^{-7}$ (s^{-2})	

isotropic growth rate. Using Equation 8, the kinetic constant, k, can be independently calculated by measuring some microstructural parameters related to N_0 and u. Under the hypothesis of complete nucleation at $t = 0$ and isotropic constant growth rate, it follows that all the growing titanate particles will have the same radius r at time t, corresponding to the radius r_{max} of the largest particle section observed on a cross section of the sample and then

$$u = \frac{r_{max}}{t} \quad (9)$$

The number of particles, N_A, per unit cross-sectional area is related to N_0 by the relationships [16]

$$N_A = 2N_0 r = 2N_0 ut \quad (10)$$

where Equation 9 was used to define the radius, r, of the monosized spheres. Equation 10 is strictly valid in the absence of impingement, i.e. $\alpha \lesssim 0.2$. Microstructural observations corresponding to different reaction times were carried out. Both u and N_0 were found approximately constant with time, as shown in Figs 6 and 7, supporting titanate formation by growth at constant rate from N_0 initial nuclei. The average values of N_0, u and the corresponding values of k calculated from Equation 8 are reported in Table III. The value of N_0 is the same for both samples ($x = 0$ and 10^{-3}) despite the expected increase of the density of nuclei at $x = 10^{-3}$. However, the standard deviation of N_0 is quite large and might hide a small difference. The calculated values of k (Table III) are in good agreement with the values coming from the Avrami fit of the data (Table II). Different mechanisms can be a priori formulated to explain the formation of Al_2TiO_5 in a heterogeneous matrix: gas-phase transport, titanium transport through Al_2O_3 particles or at the Al_2O_3 surface/interface, aluminium transport through TiO_2 particles or at TiO_2 surface/interface and transport through Al_2TiO_5. Because at 1300 °C the partial pressure of both TiO_2 and Al_2O_3 ($p_{TiO_2} \approx 10^{-6}$ Pa [17], $p_{AlO_2} \approx 10^{-11}$ Pa [18]) as well as the diffusivity of titanium in Al_2O_3 ($\approx 10^{-18}$ $m^2 s^{-1}$ [19]) and the parabolic rate constant of Al_2TiO_5 ($\approx 10^{-17}$ $m^2 s^{-1}$ [4]) are too low to sustain the observed growth rate, only aluminium transport through TiO_2 or at interfaces can be responsible for Al_2TiO_5 particle growth, in agreement with other work [3, 20]. As the growth of Al_2TiO_5 nodules occurs in a Al_2O_3–TiO_2 matrix of fine particles (0.5–3 μm), the diffusion distance remains approximately constant throughout the reaction. leading to constant growth rate even in the presence of solid-state diffusion-controlled growth. An order of magnitude estimate of the effective aluminium diffusion coefficient in TiO_2 of $10^{-12.2 \pm 0.5}$ $m^2 s^{-1}$ can be obtained from the aluminium flux corresponding to the observed growth rate of 5.5 ± 0.6 $m s^{-1}$, assuming a mean diffusion length of 2 ± 1 μm (TiO_2 particle diameter from polished sections) and a concentration difference of $\approx 1 \pm 0.5$ cation % [21] between the Al_2O_3/TiO_2 metastable interface and the Al_2O_3/Al_2TiO_5 interface. This figure can be compared with the aluminium diffusivity in niobium-doped polycrystalline TiO_2 at 1300 °C: 1.2×10^{-11} $m^2 s^{-1}$ [22].

3.2.2. Samples with composition $x = 10^{-2}$

At intermediate $MgAl_2O_4$ content ($x = 0.01$) the regression analysis yields $m = 1.7$ for standard samples and $m = 1.9$ for presintered samples (Table II), with

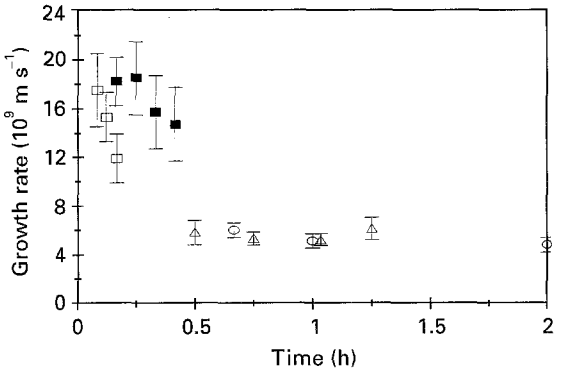

Figure 6 Average growth rate of Al_2TiO_5 nodules versus time. x: (○) 0, (△) 0.001, (□) 0.01, (■) 0.01 presintered.

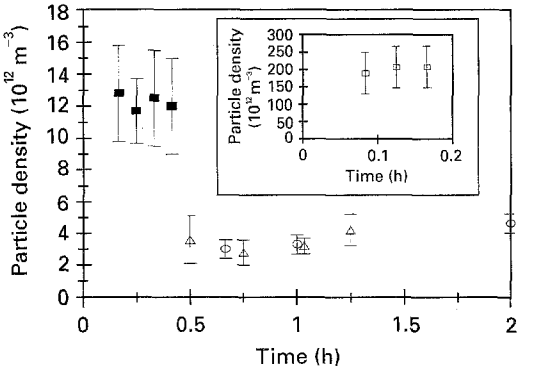

Figure 7 Al_2TiO_5 particle density versus time. x: (○) 0, (△) 0.001, (□) 0.01, (■) 0.01 presintered.

TABLE III Average values of u, N_0 and k calculated using Equations 8–10 and 12

	x			
	0	10^{-3}	10^{-2}	10^{-2} presintered
u ($m s^{-1}$)	$5.3 \pm 0.6 \times 10^{-9}$	$5.6 \pm 0.6 \times 10^{-9}$	1.5×10^{-8}	1.7×10^{-8}
N_0 (m^{-3})	$3.6 \pm 0.7 \times 10^{12}$	$3.5 \pm 0.7 \times 10^{12}$	$1.9 \pm 0.6 \times 10^{14}$	$1.2 \pm 0.3 \times 10^{13}$
k	$2.2 \pm 1 \times 10^{-12}$ (s^{-3})	$2.6 \pm 1 \times 10^{-12}$ (s^{-3})	$5 \pm 2 \times 10^{-5}$ ($s^{-3/2}$)	$5 \pm 2 \times 10^{-8}$ (s^{-2})

evidence of a different growth mechanism in comparison to $x = 0$ and 10^{-3}. Such a variation cannot be ascribed to a different morphology of the growing particles ($m = 2$ for plate-like particles) as they remain approximately spherical, nor to diffusion-controlled growth with parabolic kinetics ($m = 1.5$), as development of a barrier layer around Al_2TiO_5 nodules was not observed within the limits of SEM resolution. However, the presence of a glassy phase film, as observed in both pure and MgO-stabilized Al_2TiO_5 [23], cannot be excluded. Assuming again growth from N_0 initial nuclei, Equations 9 and 10 can be still used to calculate the average growth rate between $t = 0$ and the generic time t and the corresponding density of nuclei. The results are shown in Figs 6 and 7 and the average values are reported in Table III. The growth rate is about three times higher than at $x = 0$ and 10^{-3}. Both standard and presintered samples, despite the large standard deviation of the measures, exhibit a significant decrease of the average growth rate with time. The corresponding density of nuclei is approximately constant and increases in comparison with the value found at $x = 0$ and 10^{-3} by a factor about 50 for standard samples and by a factor of about 3.5 for presintered samples, further supporting the creation of additional nuclei related to spinel addition. Equation 8 is no longer valid in the presence of a time-dependent growth rate. As a consequence, the time exponent, m, in the Avrami Equation 6 will take values different from those corresponding to constant growth rate. In the present case, assuming that the radius of the growing particles can be described by

$$r = Ct^n \qquad \tfrac{1}{2} \leqslant n \leqslant 1 \tag{11}$$

the general expression of the volume fraction of the new phase, under the hypothesis of complete nucleation at $t = 0$, will be (see Appendix)

$$\beta = 1 - \exp(-kt^m)$$
$$= 1 - \exp(-\tfrac{4}{3}\pi N_0 C^3 t^m);\ m = 3n,\ \tfrac{3}{2} \leqslant m \leqslant 3 \tag{12}$$

The case $m = 3$ corresponds to the usual condition of constant growth rate, whereas the case $m = 3/2$ is formally equivalent to diffusion-controlled growth with a parabolic rate law. Optimal values (in the least squares sense) of C and n can be obtained by fitting the experimental radius data versus time. However, considering the limited number of available data, the results represent only a rough estimate. For standard samples it is $n = 0.46 \pm 0.1$ and $C = 4 \times 10^{-7}$. Considering the standard deviation, it can be assumed $n \simeq 0.5$, which corresponds to $m = 1.5$, close to the value 1.7 obtained from the overall kinetics (Table II). The value of k, calculated from Equation 12, $5 \times 10^{-5}\ s^{-3/2}$ is in good agreement with the value $4 \times 10^{-5}\ s^{-3/2}$ obtained from the overall kinetics (Table II). For presintered samples it is $n = 0.75 \pm 0.1$ and $C = 1 \times 10^{-7}$. Assuming $n = 2/3$ results in $m = 2$, close to the value $m = 1.9$ obtained from the overall kinetics. The corresponding value of k is $5 \times 10^{-8}\ s^{-2}$, to be compared with the value $1.2 \times 10^{-7}\ s^{-2}$ of Table II. Although the present approach is completely empirical, it nevertheless allows a general expression to be defined of the kinetic constant k, valid even when $m < 3$, which leads to values in reasonable agreement with those obtained from the overall kinetics. The reasons for the different behaviour of the growth rate in comparison to samples $x = 0$ and 10^{-3} are not clear. It is possible, however, to consider some different effects to explain qualitatively the experimental results. Small cations such as Co^{2+}, Fe^{2+}, Mg^{2+} and Al^{3+}, are known to diffuse rapidly along the c-axis direction of TiO_2-rutile [24, 25], compared to cation self-diffusion. The dependence of the impurity self-diffusion coefficient on the oxygen partial pressure suggests a diffusion mechanism by a mixture of interstitialcy and interstitial jumps [25] with the cooperative motion of interstitial titanium ions, which represent the dominant cationic defect in rutile. As a consequence, substitutional dissolution of magnesium impurities in rutile can increase the diffusivity of aluminium ions by creating additional interstitial titanium ions besides those arising from intrinsic disorder and Al_2O_3 dissolution

$$TiO_2 + 2MgAl_2O_4 \rightarrow 2Mg''_{Ti} + 4O^x_O + Ti_i^{\cdots} + 2Al_2O_3 \tag{13}$$

On the other hand, as the reaction occurs rapidly in a porous matrix, surface transport can represent an important contribution to the overall matter transport; however, the importance of surface diffusion is expected to decrease progressively as microstructure develops.

3.2.3. Samples with composition $x = 10^{-1}$

At the highest $MgAl_2O_4$ content ($x = 0.1$), conversion values below 0.7 are experimentally not accessible, as the reaction is too fast and fit of the available data by Equation 7 is meaningless, as it gives $m = 0.3$. Because under these conditions the titanate particle density is very high (10^{17}–$10^{19}\ m^{-3}$) and comparable with the particle density in the matrix, the reagents are rapidly separated by the growing product, and solid-state diffusion through Al_2TiO_5 is likely to play an important role in the early stages of reaction, as the diffusion distances are strongly reduced. An order of magnitude estimate of the kinetic constant corresponding to growth controlled by diffusion through Al_2TiO_5 can be obtained using a diffusion-controlled growth model for spherical geometry, such as that of Ginstling and Brounshtein [26]

$$1 - \tfrac{2}{3}\alpha - (1 - \alpha)^{\frac{2}{3}} = 2\frac{k}{R^2}t \tag{14}$$

where k is the kinetic constant, R the radius of the particle and t the reaction time. Considering that the observed diameter of the titanate particles is in the range 0.5–3 μm and that the average diameter of the original particles is ≈ 1 μm, a value of R in the range 0.25–1 μm can be assumed. After 30 min the reaction is 90% complete and only the biggest original particles remain. As a consequence, assuming $\alpha \approx 1$ in the time range 10 min to 1 h, a k value of $10^{-16.5 \pm 1}$ is obtained. This value can be compared with

$k = 10^{-17.2 \pm 0.8}$ at 1302 °C and $k = 10^{-16.2 \pm 0.5}$ at 1362 °C obtained by Freudenberg and Mocellin [4] for the growth of Al_2TiO_5 in the slow-growth regime. The results suggest that transport across the product layer contributes appreciably to the overall formation kinetics even at the beginning of reaction.

3.3. Nucleation and growth mechanism of Al_2TiO_5

Reaction 3 effectively occurs at temperatures $\geqslant 1150$ (± 25) °C and the isothermal kinetics $\alpha = f(t)$ is reported in Fig. 8 for $T = 1200$ and 1300 °C. The composition of the solid solution, calculated from the unit cell edges, results in $x = 0.5 \pm 0.03$ and remains constant as the reaction proceeds. Conversion of $MgAl_2O_4$ and TiO_2 into the titanate solid solution is quite fast even at 1200 °C (60% conversion after 30 min). The reaction is much faster at 1300 °C, being 80% completed after 15 min. This behaviour indicates that nucleation of the new phase is easy and not hindered by the strain-energy contribution to the overall driving force, as observed for pure Al_2TiO_5. When the reacted fraction reaches about 80%, the reaction rate strongly decreases. One possible interpretation can be related to the non-uniform particle size of the spinel powder, as the reaction rate strongly depends on the particles radius ($\approx R^{-1}$ for interface-controlled reactions, $\approx R^{-2}$ for diffusion-controlled reactions). As a consequence, finer particles convert faster than the coarser ones. In conclusion, when $MgAl_2O_4$ and TiO_2 react into the Al_2O_3–TiO_2 matrix, Reaction 3 will be able to provide, within a few minutes, a large number of $Mg_{0.5}AlTi_{1.5}O_5$ particles, which act as nuclei for subsequently titanate formation and growth. The expected number of titanate particles per unit volume, N_V, can be calculated from the volume, V_s, of spinel added per unit volume of titanate solid solution and the average size, d_s, of the spinel particles, under the hypothesis of complete nucleation at $t = 0$ and isotropic constant growth rate, assuming the formation of a titanate nodule for each spinel particle

$$N_v = \frac{V_S}{\pi d^3/6} \qquad (15)$$

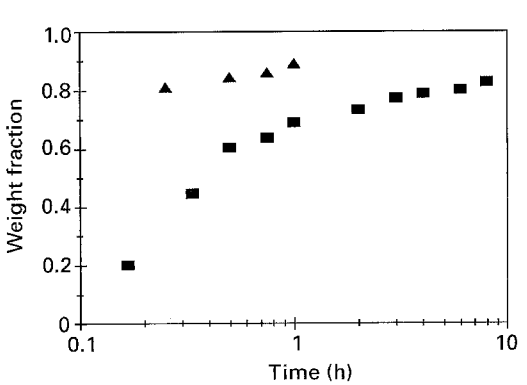

Figure 8 Isothermal kinetics of the reaction $\frac{1}{2}MgAl_2O_4 + \frac{3}{2}TiO_2 \rightarrow AlMg_{0.5}Ti_{1.5}O_5$ at (■) 1200 and (▲) 1300 °C.

The volume fraction of spinel is related to the composition of the solid solution by

$$V_S = \frac{\rho_{Al_2TiO_5} v_{MgAl_2O_4}}{M_x} x \simeq 0.81x \qquad \text{for } x \ll 1 \qquad (16)$$

where $\rho_{Al_2TiO_5}$ is the density of the titanate solid solution (3.7 g cm^{-3}), $v_{MgAl_2O_4}$ the $MgAl_2O_4$ molar volume (39.76 cm^3) and M_x the molecular weight of the solid solution. This latter can be approximated, for small values of x, to the molecular weight of Al_2TiO_5. The expected average size of the titanate particles can be simply obtained as $d_v = (6/\pi N_v)^{1/3}$. The values of N_v and d_v calculated for $d_s = 0.5$ μm are reported in Table IV together with the experimental values corresponding to the N_0 data of Table III. For $x = 0.1$, the measured number of titanate particles is comparable with that expected from the number of $MgAl_2O_4$ nuclei, whereas at smaller values of x it is about three orders of magnitude lower. Such a reduction of seed density can be related to coarsening of the $MgAl_2O_4$ particles, reaction of $MgAl_2O_4$ with impurities present in the matrix, formation of glassy phases and dissolution of $MgAl_2O_4$ in Al_2O_3 and TiO_2. In particular, the formation of a glassy phase induced by silicon impurities has been shown to reduce the amount of MgO present in the titanate solid solution [23]. The same factors are also thought to be responsible for the observed reduction of seed density after prolonged annealing at 1100 °C.

The use of different nucleating agents has also been considered; in particular $MgTi_2O_5$. This phase is isostructual with Al_2TiO_5 and formation of solid solutions occurs over the full composition range [6]. Direct formation of Al_2TiO_5 by heteroepitaxial growth on the $MgTi_2O_5$ particles is, in principle, possible without any intermediate chemical transformation, different from the case of $MgAl_2O_4$. The available thermochemical data [17] indicate spinel to be the stablest compound among the different ternary oxides in the MgO–Al_2O_3–TiO_2 system ($MgAl_2O_4$, $MgTi_2O_4$, $MgTiO_3$, $MgTi_2O_5$, Al_2TiO_5). As a consequence, when any magnesium titanate is added to an Al_2O_3–TiO_2 mixture, it spontaneously transforms into $MgAl_2O_4$ as the standard free energy of reactions

$$Mg_2TiO_4 + 2Al_2O_3 \rightarrow 2MgAl_2O_4 + TiO_2 \qquad (17)$$

$$MgTiO_3 + Al_2O_3 \rightarrow MgAl_2O_4 + TiO_2 \qquad (18)$$

$$MgTi_2O_5 + Al_2O_3 \rightarrow MgAl_2O_4 + 2TiO_2 \qquad (19)$$

TABLE IV Comparison between experimental and calculated density of nuclei and particle size (Equations 15 and 16)

	x		
	10^{-3}	10^{-2}	10^{-1}
N_v calc. (m^{-3})	1.2×10^{16}	1.2×10^{17}	1.2×10^{18}
N_v exp. (m^{-3})	3.5×10^{12}	1.9×10^{14}	10^{17}–10^{19}
d_v calc. (μm)	5.3	2.5	1.1
d_v exp. (μm)	81	22	0.5–3

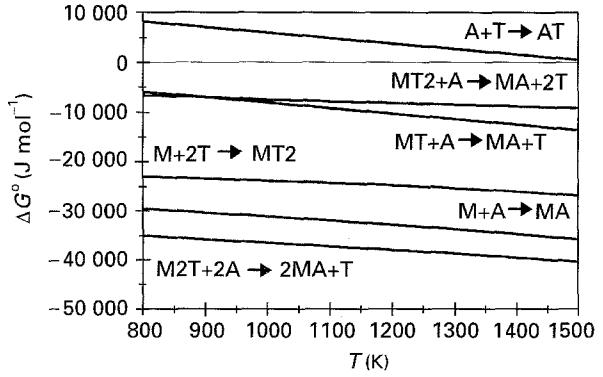

Figure 9 Standard Gibbs' free energy versus temperature for different reactions in the system Al_2O_3–TiO_2–MgO. A = α-Al_2O_3; T = TiO_2-rutile; M = MgO; AT = Al_2TiO_5; MA = $MgAl_2O_4$; M2T = Mg_2TiO_4; MT = $MgTiO_3$; MT2 = $MgTi_2O_5$.

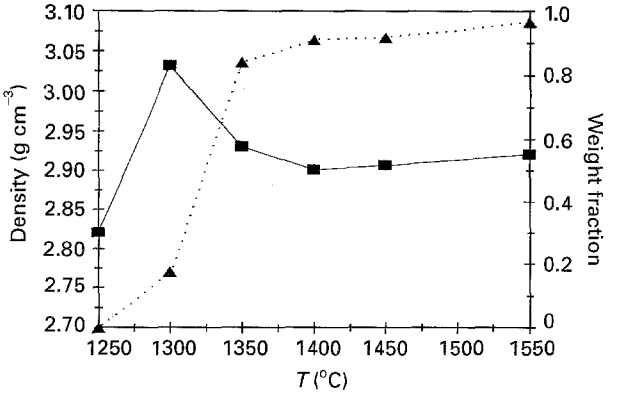

Figure 10 (▲) Fraction converted and (■) density versus temperature of samples with final composition $x = 0.01$.

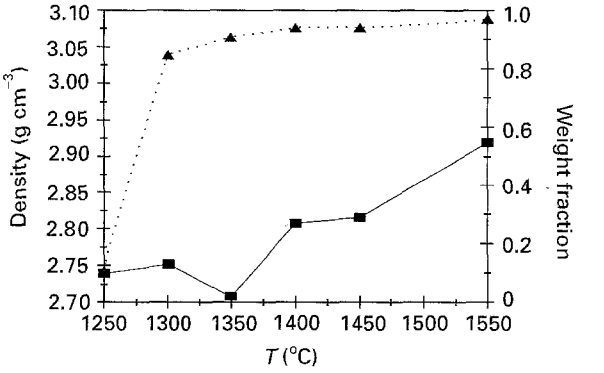

Figure 11 (▲) Fraction converted and (■) density versus temperature of samples with final composition $x = 0.1$.

is considerably negative, as shown in Fig. 9. In the case of Mg_2TiO_5, it has been experimentally verified, that Reaction 19 occurs rapidly above ≈ 1100 °C inside the Al_2O_3–TiO_2 mixture. The presence of TiO_2 is of fundamental importance in that the stoichiometric $MgTi_2O_5$–Al_2O_3 mixture reacts at very low rate; after 8 h at 1100 °C no $MgAl_2O_4$ was detected.

Magnesium impurities are always present in commercial Al_2O_3 powders and because MgO solubility in Al_2O_3 is very limited even at high temperature (no more than some tenths p.p.m. at 1300 °C [27, 28]), spinel can either be present in the starting material or formed during heating. As a consequence, some of the "easy to nucleate" sites of unknown nature which are responsible for the nucleation of "pure" aluminium titanate [3, 5] have to be associated with $MgAl_2O_4$ crystallites. The active nuclei for titanate growth, consisting of $MgTi_2O_5$–Al_2TiO_5 solid solution, are later formed through Reaction 3.

4. Al_2TiO_5 formation under non-isothermal conditions

The fraction of Al_2TiO_5 and the apparent density of samples with $x = 0.01$ heated to different temperatures (1250, 1300, 1350, 1400, 1450 and 1550 °C) at 1 °C min^{-1} and then rapidly cooled down are shown in Fig. 10. The density can be correlated to titanate formation and sintering because Al_2TiO_5 has a lower density (3.7 g cm^{-3}) in comparison with the equimolar Al_2O_3/TiO_2 mixture (4.1 g cm^{-3}). Below 1300 °C, no formation of titanate occurs and density increases as sintering of the Al_2O_3/TiO_2 matrix proceeds. Between 1300 and 1350 °C, titanate formation occurs by rapid growth of the Al_2TiO_5 crystals and density accordingly decreases. Above 1350 °C, the titanate formation rate slows down, as the reaction involves conversion of the residual Al_2O_3 and TiO_2 particles via solid-state diffusion through Al_2TiO_5 and density slightly increases due to limited sintering. In Fig. 11 the same kinds of data are reported for the case $x = 0.1$. Reaction starts at lower temperature, as it involves the formation of $MgTi_2O_5$–Al_2TiO_5 solid solution. The expansion of the specimen is limited, indicating the formation of fine particles which begin to sinter at 1300–1350 °C. Above 1350 °C, titanate formation is almost complete and sintering becomes the prevailing process. At difference with $x = 0.01$, the densification rate is much greater due to the formation of finer titanate particles.

5. Conclusions

The solid-state reaction between Al_2O_3 and TiO_2 fine powders of moderate purity has been studied at 1300 °C in the presence of different amounts of $MgAl_2O_4$ corresponding to different compositions of the final product $Al_{2(1-x)}Mg_xTi_{(1+x)}O_5$: $x = 0$, 10^{-3}, 10^{-2} and 10^{-1}. The experimental results suggest the following conclusions.

1. The conversion of parent oxides becomes increasingly fast as the amount of added spinel increases.
2. Two different reaction stages were identified when $x \leqslant 0.01$: the initial nucleation and rapid growth of approximately spherical titanate nodules and the final slow conversion of the residual Al_2O_3 and TiO_2 particles trapped during the rapid growth by solid-state diffusion through Al_2TiO_5. The initial stage can be described in terms of the Avrami kinetic equation with nucleation at $t \simeq 0$ of all titanate nodules and the reaction is probably controlled by aluminium transport through TiO_2.
3. When $x = 0.1$ only one reaction stage was identified; solid-state diffusion through Al_2TiO_5 becomes important even at the beginning of the reaction.

4. As the amount of added $MgAl_2O_4$ increases, a larger density of nuclei is available for titanate formation. The initial nuclei are probably constituted of $Mg_{0.5}AlTi_{1.5}O_5$ and formed by reaction between spinel and TiO_2.

5. Reaction sintering of Al_2TiO_5 in the presence of MgO, $MgAl_2O_4$ or $Mg_2Ti_2O_5$ represents a method to obtain sintered materials with controlled microstructure.

The present results provide, in addition, new information about solid-state reactivity in the ternary system Al_2O_3–TiO_2–MgO.

Appendix

For random nucleation throughout the volume of the sample, the general expression of the volume fraction, β, of transformed material at time, t, is [15]

$$\beta = 1 - \exp\left[- \int_0^t v_\tau \, {}^vI \, d\tau \right] \quad \text{(A1)}$$

where v_τ is the volume at time t of transformed region nucleated at time τ and ${}^vI$ the nucleation rate per unit volume. Using Equation 11, the transformed volume will be expressed as

$$v_\tau = \tfrac{4}{3}\pi C^3 (t - \tau)^m, \quad m = 3n \quad (t > \tau) \quad \text{(A2)}$$

As a first approximation, it will be assumed that, at $t = 0$, there are N_0 sites per unit volume which will be exhausted at an early stage of reaction. As a consequence, Equation A1 reduces to

$$\beta = 1 - \exp[- \tfrac{4}{3}\pi N_0 C^3 t^m] \quad \text{(A3)}$$

When $n = 1$, $m = 3$ and Equation A3 is equivalent to the Avrami equation. When $n < 1$, $m < 3$; for example $n = 2/3$ corresponds to $m = 2$.

References

1. P. STINGL, J. HEINRICH and J. HUBER, in "Proceedings of the 2nd International Symposium on Ceramic Materials and Components for Engines", Lübeck-Travemünde, FRG, April 1986, edited by W. Bunk and H. Hausner (DKG, Bad Honnef, 1986) p. 369.
2. E. KATO, K. DAIMON and J. TAKAHASHI, *J. Am. Ceram. Soc.* **63** (1980) 355.
3. B. FREUDENBERG and A. MOCELLIN, *ibid.* **70** (1987) 33.
4. *Idem, ibid.* **71** (1988) 22.
5. V. BUSCAGLIA, P. NANNI, G. BATTILANA, G. ALIPRANDI and C. CARRY, *J. Eur. Ceram. Soc.* **13** (1994) 419.
6. M. ISHITSUKA, T. SATO, T. ENDO and M. SHIMADA, *J. Am. Ceram. Soc.* **70** (1987) 69.
7. H. A. J. THOMAS, R. STEVENS and E. GILBART, *J. Mater. Sci.* **26** (1991) 3613.
8. G. TILLOCA, *ibid.* **26** (1991) 2809.
9. H. WOHLFROMM, J. S. MOYA and P. PENA, *ibid.* **25** (1990) 3753.
10. V. BUSCAGLIA, P. NANNI, G. BATTILANA, G. ALIPRANDI and C. CARRY, *J. Eur. Ceram. Soc.* **13** (1994) 411.
11. V. BUSCAGLIA, M. ALVAZZI DELFRATE, P. NANNI, M. LEONI and C. BOTTINO, in "Proceedings of the 8th CIMTEC-World Ceramic Congress and Forum on New Materials", Florence, June 1994, edited by P. Vincenzini (Techna, Faenza, Italy) **3C**, p. 1867
12. R. W. G. WYCKOFF, "Crystal Structures", Vols 1 and 3 (Krieger, Malabar, FL, 1981).
13. B. MOROSIN and R. W. LYNCH, *Acta Crystallogr. B* **28** (1972) 1040.
14. C. E. HOLCOMBE Jr, and A. L. COFFEY Jr, *J. Am. Ceram. Soc.* **56** (1973) 220.
15. J. W. CHRISTIAN, "The theory of transformations in metals and alloys", Part I (Pergamon Press, Oxford, 1981) Ch. 12.
16. E. E. UNDERWOOD, "Quantitative stereology" (Addison Wesley, Reading, 1970) p. 91.
17. O. KNACKE, O. KUBASCHEWSKI and K. HESSELMANN, "Thermochemical properties of inorganic substances" (Springer, Berlin, 1991).
18. M. W. CHASE Jr, C. A. DAVIES, J. R. DOWNEY Jr, D. J. FRURIP, R. A. McDONALD and A. N. SYVERUD, "JANAF Thermochemical Tables", 3rd Edn (National Bureau of Standards, Washington, DC, 1985).
19. R. A. LANGENSIEPEN, R. E. TRESSLER and P. R. HOWELL, *J. Mater. Sci.* **18** (1983) 2771.
20. H. WOHLFROMM, P. PENA, J. S. MOYA and J. REQUENA, *J. Am. Ceram. Soc.* **75** (1992) 3473.
21. B. FREUDENBERG, PhD thesis 709, Ecole Polytechnique Federale de Lausanne, Switzerland (1988).
22. M. F. YAN and W. W. RHODES, *J. Appl. Phys.* **53** (1982) 8809.
23. H. WOHLFROMM, T. EPICIER, J. S. MOYA, P. PENA and G. THOMAS, *J. Eur. Ceram. Soc.* **7** (1991) 385.
24. J. SASAKI, N. L. PETERSON and K. HOSHINO, *J. Phys. Chem. Solids* **46** (1985) 1267.
25. A. ATKINSON, *Adv. Ceram.* **23** (1987) 3.
26. A. M. GINSTLING and B. I. BROUNSHTEIN, *J. Appl. Chem. USSR* **23** (1950) 1327.
27. K. ANDO and M. MOMODA, *Adv. Ceram.* **23** (1987) 137.
28. S. K. ROY and R. L. COBLE, *J. Am. Ceram. Soc.* **51** (1968) 1.

Received 4 January
and accepted 8 September 1995